Laser-induced bubble generation on a gold nanoparticle: A nonsymmetrical description

Eduardo Acosta,[1] Martín G. González,[1,2,*] Patricio A. Sorichetti,[1] and Guillermo D. Santiago[1]

[1]*Grupo de Láser, Óptica de Materiales y Aplicaciones Electromagnéticas (GLOMAE), Departamento de Física, Facultad de Ingeniería, Universidad de Buenos Aires, Paseo Colón 850, C1063ACV, Buenos Aires, Argentina*

[2]*Consejo Nacional de Investigaciones Científicas y Técnicas (CONICET), C1425FQB Buenos Aires, Argentina*

(Received 27 April 2015; revised manuscript received 22 June 2015; published 1 December 2015)

The modeling of bubbles initiated by laser-irradiated nanoparticles is of interest for many applications. There is at present no comprehensive physical picture for all the stages of the process. We present an alternative approach with a key assumption: the vapor bubble evolves adjacent to the nanoparticle. To take into account the irreversible evolution, the statistical rate theory was used, thus avoiding the introduction of extra ad hoc parameters. Model results agree well with published data and our measurements. The only free parameter, the thermal boundary conductance, can be obtained by adjusting the model to the experimental data.

DOI: 10.1103/PhysRevE.92.062301 PACS number(s): 64.70.fh, 05.70.Np, 82.60.Qr

I. INTRODUCTION

Gold nanoparticles (GNPs) can be used as active components in many biophotonic applications [1–3]. Their extinction cross section can be four to five orders of magnitude higher than that of conventional dyes, leading to efficient heating [4]. Since the size of the cells is in the micron and submicron range, the use of NPs allows strongly localized heating processes and the manipulation and destruction of cellular structures [5].

Recent experiments have attempted to characterize the kinetic and thermodynamic aspects of nanobubble formation around heated GNPs [6–9]. However, there is at present no clear physical picture of bubbles formation and implosion, or of the roles of symmetry and thermal boundary conductance.

When a GNP that is initially at thermal equilibrium with its surroundings is heated by a laser pulse, the temperature of the fluid that is in thermal contact with the GNP increases. At the critical fluence F_c, the fluid nears the kinetic temperature, and the conditions for a phase change are met. A fluence larger than F_c leads to the formation of a nanobubble (NB).

Most of the previous works [10–16] assumed that, once the NB forms, it is completely surrounded by the vapor layer [symmetrical model (SM)]. This hypothesis does not take into account that, since gold-liquid and gold-vapor thermal couplings differ in several orders of magnitude, the NP is decoupled from the water. Therefore, the vapor mass of the NB cannot increase; it continues evolving and eventually collapses. Given a laser pulse with a fluence larger than F_c, the main parameters of the SM that determine the lifetime τ_b and the maximum thickness $\delta_{b\max}$ of the NB are the thermal boundary conductance, G, and the time it takes to evaporate the fluid, τ_{cL}. For a pulse duration around 5 ns, $G \approx 120\,\mathrm{MW/m^2\,K}$, and $\tau_{cL} \approx 1$ ps (twice the time between collisions of molecules of water), an estimate of τ_b and $\delta_{b\max}$ returns values around 0.1 ns and 5 nm, respectively. Thus, multiple small bubbles should be observed from a single pulse. Nevertheless, experimental data [6–9] show a large single NB.

In contrast, we propose an asymmetrical model (AM) in which it is assumed that the phase change in the fluid begins at some point on the NP surface, and then the NB grows adjacent to it (Fig. 1, top). The heating stage, which determines F_c, is the same as in the SM. The difference between the AM and the SM begins in the nucleation stage. The SM considers the NP to be thermally isolated by the NB (that evolves adiabatically). In contrast, the AM does not consider the NB to be an isolated system; it exchanges energy and mass through its boundary (with the liquid) and the region in contact with the NP. When the energy flow through the NP surface is not large enough to maintain the surrounding liquid temperature at the boiling one, the nucleation ends and the NB starts to collapse. An additional distinctive feature of the AM is that G is the only adjustable parameter, and can be obtained by fitting the model to experimental data.

II. MODEL

For modeling purposes the evolution of the NB can be described in two stages: (i) heating of the particle and surrounding liquid, and (ii) formation (nucleation) and evolution of the NB.

The model considers a spherical NP of radius R_p in water and initially in thermal equilibrium at temperature T_0. The particle is located at the coordinate origin and illuminated with a laser pulse with a beam diameter much larger than R_p, fluence F, and Gaussian temporal profile of width, τ. The power absorbed by the NP, $Q(t)$, is related to the laser intensity $I(t)$ and the absorption coefficient σ. The latter depends on the size, shape and material properties of the NP, and can be computed with Mie's theory. Part of the absorbed energy heats up the NP, and the rest is delivered to the water. The optical energy absorbed by the fluid may be neglected. Owing to the high thermal conductivity of metals and the small size of the NP, we set the same temperature at every point of the NP, provided the laser pulse is longer than 0.1 ns [17].

The heating of the NP depends on the coupling with its surroundings. Since NPs are very small, G plays an important role on the thermal evolution [18].

When G is large, the interface effects can be neglected and the temperature of the NPs is almost equal to that of the medium [19]. On the other hand, when the interface effects cannot be neglected, the cooling rate is limited by the surface thermal resistance [20]. Based on the latter, we use the

*Author to whom all correspondence should be addressed: mggonza@fi.uba.ar

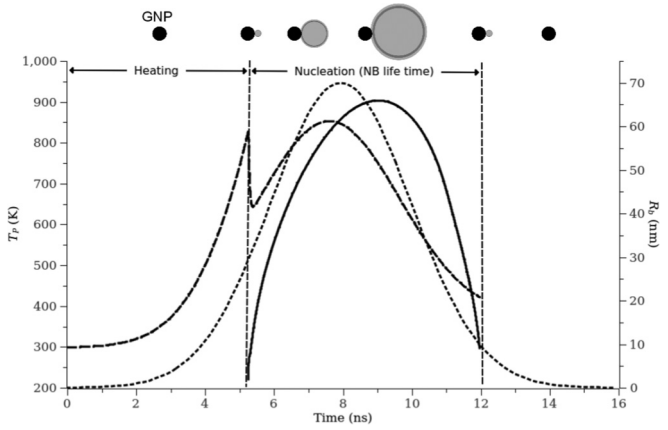

FIG. 1. Top: pictorial NB time evolution. Black disk, GNP; gray circle, NB. The pictures show the relative sizes of the NP and the NB. Bottom: time evolution of the NB radius (solid), T_p (dashed), and laser intensity (dotted). $G = 180\,\mathrm{MW/m^2\,K}$, $R_P = 6.65\,\mathrm{nm}$, $F = 5\,\mathrm{kJ/m^2}$, $\tau = 4.8\,\mathrm{ns}$.

following set of equations [20] to obtain the evolution of the temperatures of the NP (T_p) and the liquid (T_L) respectively:

$$m_p\, C_p\, dT_p(t)/dt = Q(t) - 4\pi R_p^2\, G\,(T_p(t) - T_L(r = R_p, t)) \tag{1}$$

$$4\pi R_p^2\, G\,(T_p(t) - T_L(r = R_p, t)) = -4\pi R_p^2 k_L \left.\frac{\partial T_L}{\partial r}\right|_{r=R_p} \tag{2}$$

$$\rho_L C_L \frac{\partial T_L}{\partial t} = \vec{\nabla}\,(k_L \vec{\nabla} T_L) + q_L(t) \tag{3}$$

where m_p and C_p are the mass and specific heat of the NP, respectively, and ρ_L, C_L and k_L are the density, specific heat, and thermal conductivity of the liquid. q_L is the power per unit volume absorbed by the liquid.

When a liquid is heated beyond the boiling point, a sudden phase change develops, leading to a rapid vaporization. The temperature T_k at which this process happens is equal to that of the vapor when the nucleation stage begins. This can be qualitatively understood by applying the classic bubble-nucleation theory [21]. When the liquid reaches a temperature above the value of liquid/vapor equilibrium, the spontaneous formation of a bubble of radius R_k in conditions of mechanical equilibrium becomes possible. Symmetry breaking appears since the conditions for the generation of such a bubble are valid within a spherical shell of thickness R_k around the NP. Therefore, using this theory T_k and R_k can be estimated.

Nucleation starts with the formation of the protobubble adjacent to the NP surface. Several authors neglect evaporation and condensation during the evolution of the NB [10–16,19]. In contrast, we take into account the effects of evaporation and condensation of the fluid; therefore the vapor mass in the NB is not constant.

The thermal power transferred to the fluid surrounding the NP keeps the fluid's temperature in contact with the NP unchanged and increases the vapor mass inside the NB. Consequently, the following equation must be satisfied:

$$h_{LV} dm_{Vp}/dt = 4\pi R_p^2 G(T_p(t) - T_L(r = R_p, t_1)) - 4\pi R_p^2 k_L \partial T_L/\partial r\big|_{r=R_p} \tag{4}$$

where h_{LV} is the water vaporization enthalpy and m_{Vp} is the vapor mass produced by the NP. Before nucleation starts, the liquid's temperature in contact with the NP rises up to the kinetic limit. Once some instability triggers the nucleation, the temperature drops and stays at the boiling value (373.15 K).

The NB radius R_b increases due to the increment of m_{Vp} in a non-equilibrium state. The pressure excess causes the evolution of the NB size; this can be described by the equations of Laplace and Rayleigh-Plesset [22]. $\dot{\mathrm{R}}_\mathrm{b}$ is related to $\ddot{\mathrm{R}}_\mathrm{b}$ and the rate of change of the vapor mass in the NB, dm_b/dt, by [19].

$$\dot{R}_b = \int_{t_1}^{t} \ddot{R}_b dt + \left(4\pi R_b^2 \rho_V\right)^{-1} dm_b/dt \tag{5}$$

dm_b/dt is the sum of two processes: dm_{Vp}/dt (evaporation of liquid on the NP surface) and dm_{ec}/dt (evaporation-condensation on the NB surface). dm_{Vp}/dt is calculated using (4). Alali *et al.* [23] used the classical theory of evaporation-condensation to estimate dm_{ec}/dt. However, in that case there are some parameters whose values must be chosen ad hoc [24]. To avoid this, we calculate dm_{ec}/dt using the statistical rate theory (SRT) developed by Ward *et al.* [25] to describe the thermodynamics of an evaporating system. The SRT is used even when there is no thermal equilibrium between the translational and vibrational degrees of freedom of the fluid molecules. It is interesting to note that SRT has been successfully used to study many non-equilibrium processes, such as the excitation of molecular lasers.

dm_{ec}/dt for a spherical surface is:

$$\frac{1}{4\pi m_L R^2}\frac{dm_{ec}}{dt} = 2\,K_e\,\sin h\left(\frac{\Delta s_{LV}}{k_b}\right) \tag{6}$$

where ΔS_{LV} and K_e depend explicitly on the physicochemical properties of the system:

$$\frac{\Delta S_{LV}}{k_b} = 4\left(1 - \frac{T_V}{T_L}\right) + \left(\frac{1}{T_V} - \frac{1}{T_L}\right) \times \sum_{i=1}^{3}\left[\frac{T_i}{2} + \left(\frac{T_i}{\left(\exp\left(\frac{T_i}{2T_V}\right) - 1\right)}\right)\right] + \left(\frac{v_L}{k_b T_L}\right)(P_L - P_{SAT}(T_L)) + \ln\left(\left(\frac{T_V}{T_L}\right)^4 \frac{P_{SAT}(T_L)}{P_V}\right) + \ln\left(\frac{q_{\mathrm{vib}}(T_V)}{q_{\mathrm{vib}}(T_L)}\right) \tag{7}$$

$$q_{\mathrm{vib}}(T) = \prod_{i=1}^{3} \exp\left(-\frac{T_i}{2T}\right) \Big/ \left(1 - \exp\left(-\frac{T_i}{T}\right)\right) \tag{8}$$

$$K_e = P_V^e/\sqrt{2\pi m k_b T_L} \tag{9}$$

with $T_1 = 2306$ K, $T_2 = 5278$ K, and $T_3 = 5430$ K. k_b is the Boltzmann constant, v_L is the molecular volume of the liquid, and the subscript "sat" refers to saturation variables.

It is important to remark that, since the vapor temperature T_V differs from T_L and the vapor-liquid interface is curved, the values of the pressure P_V and the density ρ_V within the NB differ from the saturation values [26]:

$$P_V^e = P_{SAT}\ \exp\left(\frac{v_L}{k_b T_L}(P_L - P_{SAT})\right) \tag{10}$$

From the internal energy of the NB, the temporal evolution of T_V results:

$$E(\rho_V, T_V) = m_V u_V(\rho_V, T_V) = \frac{4\pi}{3} R_b^3\ \rho_V\ u_V(\rho_V, T_V) \tag{11}$$

where u_V is the internal energy per unit of vapor mass. Furthermore, the change of the internal energy can be calculated as:

$$\frac{dE}{dt} = -(P_V - P_L)\frac{dV_b}{dt} + u_V \frac{dm_b}{dt} \tag{12}$$

where V_b is the NB volume and P_L the pressure of the liquid on the NB surface.

This set of equations allows us to calculate the time evolution of T_p, T_L, m_V, E, V_b and $\dot{R}_b$. From these values we can estimate other parameters that describe the nucleation stage.

The nucleation stage ends when $dm_{V_p}/dt = 0$ and the energy flow through the NP surface is not large enough to maintain constant $T_L(r = R_p) = 373.15$ K. We assume that, when R_b decreases, the NB remains attached to the NP by short-range interfacial forces in the contact zone between the NB and the NP.

It must be remarked that at high fluence values the NP melts; therefore, the model takes into account that the solid-liquid boundary thermal conductance, G_{solid} differs from the liquid-liquid value, G_{liquid}.

III. NUMERICAL SIMULATIONS

The system of equations was solved by the method of finite differences. The thermodynamic properties of water as a function of temperature and density were calculated according to IAPWS (2009) [27]. The properties of gold were obtained from [28]. Algorithms that describe the temporal evolution of the temperature of the water were verified in two situations whose analytical solutions are known. In both cases the numerical error was less than 3% using $D_L\ \Delta t/\Delta r^2 \leqslant 0.25$, where D_L is the thermal diffusion of water and Δt and Δr are the time and spatial steps, respectively.

Figure 1 shows the time evolution of the NP temperature and the NB radius, calculated for $R_p = 6.65$ nm, $G = 180$ MW/m^2 K, and $F = 4$ kJ/m^2. During heating, T_p increases exponentially until nucleation begins. The sudden drop shows the already mentioned condition $T_L(r = R_p) = 373.15$ K. Afterward, since part of the energy is used to produce the state change, the increment rate of T_p diminishes. When the laser intensity is maximum, T_p begins to decrease. The calculation stops when the heat transfer is insufficient to maintain the temperature of the layer of water surrounding the NP.

From the calculations, it turns out that F_c is almost independent of G, and, in agreement with [29], F_c and T_k depend on τ. Moreover, the T_k values obtained were a few degrees below the kinetic temperature.

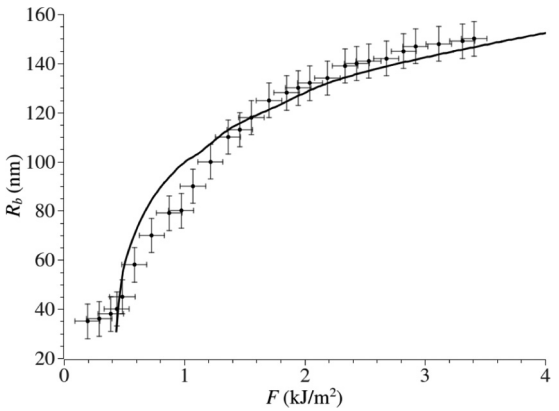

FIG. 2. NB radius vs fluence. Solid line, calculated; black dots, data from [20].

As a first validation, Fig. 2 compares the computed values of R_b versus F with the experimental results of [20] using the same input values ($R_p = 30 \pm 4$ nm, $\tau = 3$ ns, $\lambda = 355$ nm, $T_0 = 298$ K), and $G_{\text{solid}} = 180$ MW/m^2 K.

As another test, we used the data from [8], where NP of radii 15 and 50 nm were irradiated with laser pulses [$\lambda = 532$ nm, $\tau = 10$ ns, $F = (9 \pm 1)$ kJ/m^2, and $F = (5.5\ \pm 0.5)$ kJ/m^2]; the NB lifetimes were (17 ± 3) and (28 ± 16) ns. In our model, setting $G_{\text{solid}} = 180$ MW/m^2 K returns NB lifetimes of (19 ± 1) and (24 ± 1) ns. The ± 1 ns arises from the uncertainty in the fluence.

IV. EXPERIMENTAL RESULTS

We prepared spherical GNP ($R_p = 6.65$ nm) following [30]. Their size was verified by transmission electron microscopy (TEM) (size dispersion about 0.75 nm). Acoustic measurements at different fluence employed a setup similar to [31], using a frequency-doubled, Q-switched Nd:YAG laser (Continuum Minilite I, 520 nm, 4.8 $\pm$ 2 ns, 10 Hz). A plano-convex lens (30 mm focal length) focused the beam into a 1 cm glass cuvette equipped with a calibrated piezoelectric sensor [32,33]. The amplified signals were captured with an oscilloscope (Tektronix TDS 2024, 2 GS/s, 200 MHz). The laser energy was monitored with a pyroelectric detector, and τ was measured using a photodiode.

The far-field acoustical signal is:

$$P_S(r, t) = \frac{R(t_r)}{r}\left[(P_L(t_r) - P_0) + \frac{1}{2}\rho_L \dot{R}_b^2(t_r)\right] \tag{13}$$

where $t_r = t - r/c_L$ and c_L is the sound speed. Equation (13) describes the overpressure on the fluid surrounding the NB added to the effect of the NB expansion.

Since the signal bandwidth is much larger than that of the sensor, the output is proportional to its impulse response per unit area:

$$J = \int_0^\infty P_S(r, t)dt \tag{14}$$

Figure 3 shows the normalized sensor output versus the fluence. The calculated value $F_c = 2.25$ kJ/m^2 lies within the

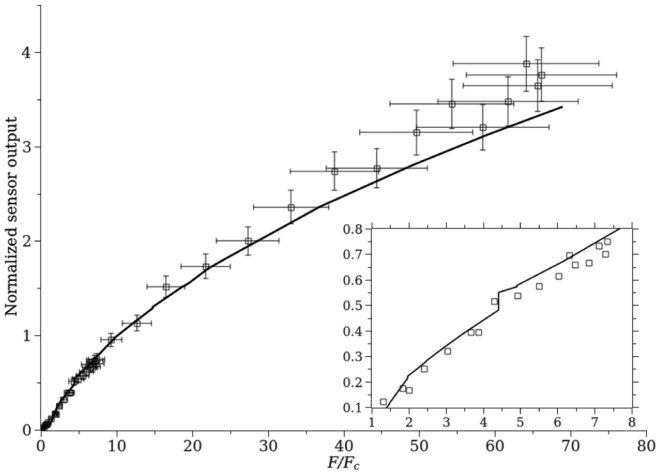

FIG. 3. Sensor output (normalized to $F = 10F_c$) vs fluence (normalized to F_c). Solid line, calculated; squares, measured; normalization values, $J_{\text{model}} = 28.5\,\text{Pa s}$, $J_{\text{measured}} = 12.9\,\text{Pa s}$.

confidence interval of the experimental $F_c = 2.5\,\text{kJ/m}^2$ with the same trend in both curves.

Experimentally, J initially increases with the fluence (until $F/F_c = 70$) and then decreases. If the fluence is then reduced, the values of J differ from those previously measured. This behavior at high values of F/F_c may be understood as a consequence of an irreversible change due to the vaporization of the NP [34]. On the other hand, a sudden increase in J is observed when F/F_c exceeds 4 (see the inset in Fig. 3). It must be stressed that in this case, when F is reduced, the same values of J are obtained. This reversible trend is due to the change in G when the NP melts.

From the values of F/F_c corresponding to the fusion and vaporization of the NP, it is possible to estimate the solid-liquid and liquid-liquid thermal boundary conductances. Fitting the model to the measured values gives $G_{\text{solid}} = 180\,\text{MW/m}^2\,\text{K}$ and $G_{\text{liquid}} = 980\,\text{MW/m}^2\,\text{K}$.

V. CONCLUSIONS

We present a different approach to model laser-induced bubble generation on NPs. We assume that the phase change in the fluid begins at some point on the NP surface, and then the nanobubble grows adjacent to it. This model describes all the stages of the formation and evolution of a laser-induced NB. To determine the conditions for the onset of the nanobubble formation, we use the classical nucleation theory, a well-known and proven treatment. In the nucleation stage we apply the statistical rate theory, which provides a simple way to describe the evaporation and condensation processes across the nanobubble surface. This way, extra ad hoc parameters required by previous treatments are avoided.

Regarding the model validation, simulation results are in good agreement with the data obtained from different experimental techniques: NB lifetime [8], NB radii [20], and pressure signal (our measurements). Moreover, from the fitting of the model to the measured $J(F)$ curve, we obtain values of G_{solid} and G_{liquid} for the system NP-liquid studied in this work.

Finally, it is important to mention that this model is intended to highlight the basic issues concerning nanobubble formation, therefore we kept it as simple as possible while describing the key aspects of the process.

ACKNOWLEDGMENT

This work was supported by the University of Buenos Aires, Grants No. UBACyT 20020120100025BA and No. 20020130100346BA; and the Consejo Nacional de Investigaciones Científicas y Técnicas (CONICET), Grant No. PIP-112-201101-00676.

[1] D. Pissuwan, S. M. Valenzuela, and M. Cortie, Trends Biotechnol. **24**, 62 (2006).
[2] V. P. Zharov, E. N. Galitovskaya, C. Johnson, and T. Kelly, Lasers Surg. Med. **37**, 219 (2005).
[3] P. Sharma, S. Brown, G. Walter, S. Santra, and B. Moudgil, Adv. Colloid Interf. Sci. **123–126**, 471 (2006).
[4] P. K. Jain, I. H. El-Sayed, and M. A. El-Sayed, Nanotoday **2**, 18 (2007).
[5] D. Wen, Int. J. Hyperther. **25**, 533 (2009).
[6] T. Katayama, K. Setoura, D. Werner, H. Miyasaka, and S. Hashimoto, Langmuir **30**, 9504 (2014)
[7] E. Lukianova-Hleb, Y. Hu, L. Latterini, L. Tarpani, S. Lee, R. A. Drezek, J. H. Hafner, and D. O. Lapotko, ACS Nano **4**, 2109 (2010).
[8] D. Lapotko, Opt. Express **17**, 2538 (2009).
[9] M. Kitz, S. Preisser, A. Wetterwald, M. Jaeger, G. Thalmann, and M. Frenz, Biomed. Opt. Express **2**, 291 (2011).
[10] J. Lombard, T. Biben, and S. Merabia, Phys. Rev. Lett. **112**, 105701 (2014).
[11] J. Lombard, T. Biben, and S. Merabia, Phys. Rev. E **91**, 043007 (2015).
[12] S. Hashimoto, D. Werner, and T. Uwada, J. Photochem. Photobiol. C **13**, 28 (2012).
[13] E. P. Furlani, I. H. Karampelas, and Q. Xie, Lab Chip **12**, 3707 (2012).
[14] A. N. Volkov, C. Sevilla, and L. V. Zhigilei, Appl. Surf. Sci. **253**, 6394 (2007).
[15] X. Liu, Y. Hou, X. Liu, J. He, J. Lu, and X. Ni, Optik **122**, 1254 (2011).
[16] E. A. Brujan, Microfluid. Nanofluid. **11**, 511 (2011).
[17] H. C. Van de Hulst, *Light Scattering by Small Particles* (Dover, New York, 1981).
[18] G. L. Pollack, Rev. Mod. Phy. **41**, 48 (1969).
[19] T. Wu, C. H. Farny, R. A. Roy, and R. G. Holt, J. Acoust. Soc. Am. **130**, 3252 (2011).
[20] A. Siems, S. Weber, J. Boneberg, and A. Plech, New J. Phys. **13**, 043018 (2011).
[21] C. T. Avedisian, J. Phys. Chem. Ref. Data **14**, 695 (1985).

[22] M. S Plesset and S. A. Zwick, J. Appl. Phys. **25**, 493 (1954).
[23] F. Alali, I. Karampelas, Y. Kim, and E. Furlani, J. Phys. Chem. C **117**, 20178 (2013).
[24] I. Akhatov, O. Lindau, A. Topolnikov, R. Mettin, N. Vakhitova, and W. Lauterborn, Phys. Fluids **13**, 2805 (2001).
[25] C. A. Ward and G. Fang, Phys. Rev. E **59**, 429 (1999).
[26] P. Rahimi and C. A. Ward, Int. J. Thermodyn. **8**, 1 (2005).
[27] Revised Release on the IAPWS Formulation 1995 for the Thermodynamic Properties of Ordinary Water Substance for General and Scientific Use, September 2009.
[28] E. Sassaroli, K. Li, and B. O'Neill, Phys. Med. Biol. **54**, 5541 (2009).
[29] E. Y. Lukianova-Hleb, A. N. Volkov, and D. O. Lapotko, Langmuir **30**, 7425 (2014).
[30] J. Kimling, M. Maier, B. Okenve, V. Kotaidis, H. Ballot, and A. Plech, J. Phys. Chem. B **110**, 15700 (2006).
[31] M. G. Gonzalez, X. Liu, R. Niessner, and C. Haisch, Appl. Phys. Lett. **96**, 174104 (2010).
[32] M. G. Gonzalez, P. Sorichetti, and G. Santiago, Rev. Sci. Instrum. **85**, 115005 (2014).
[33] M. G. Gonzalez, P. Sorichetti, and G. Santiago, *Proceedings of the 2nd IEEE Biennial Congress of Argentina (ARGENCON 2014), San Carlos de Bariloche, Argentina* (IEEE, Piscataway, NJ, 2014), pp. 576–581.
[34] T. McGrath, A. Beveridge, and G. Diebold, Angew. Chem. Int. Ed. **38**, 3353 (1999).